Journal of Hazardous Materials 375 (2019) 281–289

Contents lists available at ScienceDirect

Journal of Hazardous Materials

journal homepage: www.elsevier.com/locate/jhazmat

# Industrial textile effluent treatment and antibacterial effectiveness of *Zea mays L.* Dry husk mediated bio-synthesized copper oxide nanoparticles

Assumpta Chinwe Nwanya[a,b,c,*], Lovasoa Christine Razanamahandry[b,c], A.K.H. Bashir[b,c], Chinwe O. Ikpo[d], Stephen C. Nwanya[e], Subelia Botha[f], S.K.O. Ntwampe[g], Fabian I. Ezema[a,b,c], Emmanuel I. Iwuoha[d], Malik Maaza[b,c]

[a] *Department of Physics and Astronomy, University of Nigeria, Nsukka, Nigeria*
[b] *UNESCO-UNISA Africa Chair in Nanosciences-Nanotechnology, College of Graduate Studies, University of South Africa, Muckleneuk ridge, South Africa*
[c] *Nanosciences African Network (NANOAFNET), iThemba LABS-National Research Foundation, 1 Old Faure road, Somerset West, PO Box 722, 7129, Somerset West, South Africa*
[d] *Sensor Lab, Department of Chemistry, University of the Western Cape, Bellville, 7535, Cape Town, South Africa*
[e] *Department of Mechanical Engineering, University of Nigeria, Nsukka, Nigeria*
[f] *Electron Microscope Unit, University of the Western Cape, South Africa*
[g] *Bioresource Engineering Research Group (BioERG), Faculty of Applied Science Department of Biotechnology Cape Peninsula University of Technology, P.O. Box 652, Cape Town, 8000, South Africa*

ARTICLE INFO

*Keywords:*
Anti-Microbial
Copper oxide
Green synthesis
Photocatalysis
*Zea mays L.*

ABSTRACT

*Zea mays L.* dry husk extract was used to bio synthesize copper oxide nanoparticles. Red coloured cubic $Cu_2O$ nanoparticles were obtained for the first time via this simple, eco- friendly, green synthesis route. The $Cu_2O$ nanoparticles were thermally oxidized to pure monoclinic CuO nanoparticles at 600 °C. The phases of the copper oxides were confirmed from the x-ray diffraction (XRD) studies. The nanoparticle sizes as obtained from high resolution transmission electron microscope (HRTEM) analysis range from 10 to 26 nm, 36–73 nm and 30 – 90 nm for the unannealed $Cu_2O$, 300 °C and 600 °C annealed CuO respectively. The values of the bandgap energies obtained from diffuse reflectance of the nanoparticles are 2.0, 1.30 and 1.42 eV respectively for the unannealed, 300 °C, and 600 °C annealed copper oxide nanoparticles. The 600 °C annealed copper oxide nanoparticles showed 91% and 90% degradation ability for methylene blue dye (BM) and textile effluent (TE) respectively under visible light irradiation. While CuO_300 is more effective to inhibit the growth of *Escherichia coli* 518,133 and *Staphylococcus aureus* 9144, $Cu_2O$ is better for *Pseudomonas aeruginosa* and *Bacillus licheniformis*. The results confirm the photo-catalytic and anti-microbial effectiveness of the copper oxide nanoparticles.

## 1. Introduction

Water is the most abundant natural resources on earth. Good public health relies largely on readily available water either for drinking, domestic use, industrial or recreational use. A good percentage of the world's population do not have access to safe water today. According to the 2018 report by World Health Organisation (WHO), 844 million people do not have basic drinking-water service, including 159 million people who depend on surface water [1]. The report further stated that globally, at least 2 billion people use drinking water sources infested with faeces and that by 2025, half of the world's inhabitants would be living in water-deprived areas. With this kind of report, there is urgent need for proper water management and wastewater treatment to meet the global demand for water. A country's economic growth and development can be enhanced with proper water supply and management, which could ultimately lead to poverty reduction.

Amongst the water contaminants, organic dyes such as methylene blue used in textile industries constitute a great hazard to human health. They have been shown to be carcinogenic and cause other diseases such as heart stroke, jaundice etc. ([2–4]). In addition, most of these dyes are designed not to be biodegradable, therefore need to be removed from effluents before being discharged into the environment [5,6]. Some of the techniques used to remove organic dyes from water are adsorption using activated carbon from various organic materials [7,8] and coagulation [9,10]. Others are reverse and forward osmosis [11–13], as well as ozonation [14]. Most of these methods are slow, inefficient and are not cost effective. Apart from dye contaminants, there are also microbial contaminants of water, which include bacteria,

* Corresponding author at: Department of Physics and Astronomy, University of Nigeria, Nsukka, Nigeria.
*E-mail address:* chinwe.nwanya@unn.edu.ng (A.C. Nwanya).

https://doi.org/10.1016/j.jhazmat.2019.05.004
Received 27 November 2018; Received in revised form 14 April 2019; Accepted 2 May 2019
Available online 03 May 2019
0304-3894/ 

viruses, and protozoa. The presence of these microbes in water may cause various gastro intestinal illnesses such as diarrhea, vomiting, and cramps [15]. One of the major public health concerns of the 20th century is the disinfection of drinking water to reduce water-borne infectious disease.

In the last few decades, metal oxide nanoparticles have been used effectively for the degradation of organic dyes in wastewater [16–18]. They are also used for antimicrobial activities [19,20]. Amongst the metal oxides nanoparticles used for the decontamination of water, copper oxide nanoparticles have shown impressive results [21–23]. This is because it is relatively cheap, has a narrow bandgap and high catalytic efficiency. A plethora of methods has been used to synthesize copper oxide nanostructures for various applications. These methods include thermal decomposition [24], atmospheric plasma jet [25], hydrothermal [26]. Other methods used are chemical bath deposition [27,28], SILAR [29] as well as electrochemical [30] amongst others. In as much as copper oxides prepared using some of these methods have shown desired properties, toxic chemicals and solvents that are dangerous to human health and the environment are used as reducing/oxidizing agents. Biosynthesis of metal oxides has been used recently to overcome the challenges posed by using chemical methods. There are only a few reports on the biosynthesis of copper oxides in the literature using various plant and micro organism extracts for a wide range of applications. Nabila and Kannabiran, [31], used the extract from *actinomycetes* to synthesize copper oxide nanoparticles for antibacterial activity against fish and human bacterial pathogens, while Aminuzzaman et al., [32], used banana peel extract and studied the photocatalytic activities of the prepared copper oxide nanoparticles. Sivaraj et al., [33], studied the antimicrobial and anticancer activity of *Acalypha indica* mediated copper oxide nanoparticles, while Yu et al., [34], used *Arbutus unedo* leaf extract and tested the synthesized copper oxide nanoparticles for in-vitro cytotoxicity against nasopharynx cancer cell lines. Larvicidal activity of copper oxide nanoparticles synthesized using *T. procumbens* leaf extract was examined against Aedes aegypti species [35]. Only few works have reported on the biosynthesis of copper oxide for waste water treatment.

Maize (*Zea mays L.*) husks otherwise known as corn husks are the modified leaves that cover the ears of *Zea mays L.* plant. They are one of the waste by-products of *Zea mays L.* However, they have been shown to be a good source of various phytochemicals such as flavonoids, saponins, alkaloids, glycosides, tannins, phenols etc. [36]. They also have medicinal, anti-inflammatory and acoustic absorbing potentials [37–39]. In this work, we used extracts from *Zea mays L.* dry husk to synthesize copper oxide nanoparticles and studied their potentials for photocatalytic degradation of industrial textile effluent, methylene blue blue as well as their antibacterial activity against *Escherichia coli, Staphyloccocus aureus, Bacillus licheniformis and Pseudomonas aeruginosa.* Therefore, this study combines the advantages of green chemistry principles with that of using sustainable resources which consequently leads to human health and environmental protection.

## 2. Materials and methods

### 2.1. Copper oxide nanoparticles synthesis

Fresh *Zea maize L.* husks were dried at 40 °C until they become brittle and then grinded into powder using a grinder. 10 g of the powder was put in 200 ml of deionise water and heated at 50–60 °C for about 2 h yielding a transparent milkish extract of pH of about 4. The extract was cooled to room temperature and then filtered twice using whatman filter paper. 2.25 g of copper II acetate monohydrate ($Cu(C_2H_3O_2)_2{\bullet}H_2O$) was added to 50 ml of the extract and stirred for about 3 min. leading to complete dissolution of the salt in the extract. The colour of the resultant solution changed from transparent milkish colour to light blue indicating the reduction of the metal salt. Red precipitates were formed at the bottom of the beaker after the solution was put on a hot plate between 70–80 °C for 2 h. From literature survey, this is the first time red coloured $Cu_2O$ nanoparticles are obtained via the green synthesis method. The precipitates were separated from the aqueous extract by decanting, and then washed several times by centrifuging to remove any residual aqueous extract that may be present. The obtained precipitates were dried at 80 °C and then annealed at 300 and 600 °C. The schematic of the synthesis procedure is given in our earlier work on copper oxide [40].

### 2.2. Copper oxide nanoparticles characterizations

A Double Beam Cary 5000 UV–vis-NIR spectrophotometer was used to obtain the optical properties of the extract as well as the copper oxide nanoparticles. An integrating sphere attachment was used to measure the diffuse reflectance. The crystal phase of the copper oxide nanoparticles were obtained using a Bruker AXS D8 diffractometer with copper anode at a wavelength of 1.540 Å at an operating voltage of 40 kV and current of 40 mA. Attenuated Total Reflection-Fourier Transform Infrared spectroscopy (ATR-FTIR) was performed on a Thermo-Nicolet 8700 FTIR spectrometer. The morphology of the copper oxide nanoparticles were studied using Scanning Electron microscope (SEM) and a Tecnai F20 High Resolution Transmission Electron Microscope (HRTEM) operated at 200 kV, equipped with an Energy Dispersive X-ray Spectrometer (EDS).

### 2.3. Copper oxide photocatalytic activity

The photocatalytic activity of the CuO nanoparticles (NPs) was studied on two types of wastewater, which include the wastewater from industrial textile effluent (TE) and the synthetic wastewater based on the methylene blue dye (BM), under visible light irradiation. The textile effluent was from the "Colorite Dyers Company" (Cape Town, South Africa) which is a clothing dyeing company. Liquid medium (n = 5) for each wastewater type were prepared with CuO NPs (n = 4) and without CuO NPs (n = 1). A mass (20 mg) of $Cu_2O$, CuO annealed at 300 °C (CuO_300), CuO annealed at 600 °C (CuO_600) and the mixture of these three forms of CuO NPs was separately added with 50 ml of TE and BM wastewater. The last liquid medium was composed only of the TE and BM wastewater and exposed to the visible light irradiation The liquid medium pH was adjusted to basic condition (pH = 9). Before contact time with visible light, the mixtures were stirred for 25 min under dark condition to build up the adsorption-desorption equilibrium. Then, the mixture was exposed to visible light irradiation under constant stirring (120 rpm) and room temperature 25 °C. At initial time ($t_0$) the absorbance measurement of BM and TE wastewater was run on the wavelength ranging from 200 to 800 nm. The initial absorbance ($A_0$) of BM and TE wastewater was measured before following the dye degradation at the unique wavelength 661 nm. TE and BM aliquots (5 mL) were taken firstly at 5 min of the contact time and then every 25 min for 3 h. The dye degradation efficiencies were calculated according to the following equation:

$$D\,(\%) = \frac{(A_0 - A_t)}{A_0} \times 100 \quad (1)$$

Where:

$A_0$ : the absorbance of the TE and BM at t = 0 min ($t_0$)

$A_t$: the absorbance of the TE and BM at time t = t (t = sampling time)

Pseudo first order kinetics of the dyes degradation were calculated by using the equation

$$ln\frac{A_t}{A_0} = kt \quad (2)$$

Where: $A_0$: the absorbance of the TE and BM at t = 0 min ($t_0$)

$A_t$: the absorbance of the TE and BM at time t = t (t = sampling time)

$k$: the constant rate of the TE and BM degradation.

### 2.4. Copper oxide antibacterial activity

In addition to the photocatalytic activity, the antibacterial activity of the CuO NPs was investigated by testing the following pathogen microorganisms: *Escherichia coli* 518133, *Staphyloccocus aureus 9144*, *Bacillus licheniformis* and *Pseudomonas aeruginosa*. Petri dish plates enriched with agar nutrient medium (15 g.L$^{-1}$) were used to cultivate 200 µl of pathogen microorganisms. The petri dishes were shaken before adding the CuO NPs according to the well diffusion method. Three wells (A, B and C) were created on the surface of the solidified agar nutrient medium. Each well is corresponded to each type of the CuO NPs (A = $Cu_2O$, B = CuO_300 and C = CuO_600). Small amounts (0.04 g) of the dried powders of each CuO NPs were added into each well. Then the petri dishes were incubated directly at 37 °C for 24 h. All steps of analysis were conducted under sterile conditions.

## 3. Results and discussions

### 3.1. Structural analysis

The XRD pattern of the copper oxide nanoparticles is shown in Fig. 1. The un-annealed copper oxide showed the formation of pure cuprite $Cu_2O$ nanoparticles which could be indexed as cubic structured $Cu_2O$ with *P n*3 *m* space group (JCPDS card no. 05-0667). Crystalline peaks corresponding to (110), (111), (200), (211), (220), (311) and (222) diffraction planes at 2θ angles of 29.5, 36.36, 42.24, 52.39, 61.31, 73.45 and 77.3° respectively were observed. Upon annealing in air at 300 °C the peaks of CuO begin to appear and complete transformation to pure CuO is observed after annealing at 600 °C for 2 h as shown in the figure. The figure indicates that the CuO nanoparticles could be indexed as base-centered monoclinic CuO (space group C2/c) crystal structure (JCPDS card no. 00-048-1548). Some of the characteristics peaks are observed at 2θ angles of 32.45, 35.47, 38.63, 46.34, 48.78, 53.44, 58.21, 61.51, 66.20, 68.0, 72. 34, 75.16, 80.41 and 82.88° and are assigned respectively to the (110), (002), (111), (11-2), (20-1), (020), (202), (11-3), (31-1), (113), (311), (22-2), (11-4 and (312) diffraction planes. The thermal oxidation of $Cu_2O$ to CuO agrees with the studies of Zhu et al., [39] which is based on the activation energy for the oxidation of $Cu_2O$ following a logarithmic law. However, in our case, the phytochemicals present in the extract used in the synthesis of the copper oxide may have caused the reduction of the temperature required for the complete thermal oxidation of $Cu_2O$ to CuO leading to the formation of a pure CuO at temperature of 600 °C. The calculated crystal sizes using the Scherrer equation are 34.8, 5.5 and 22.9 nm respectively for the unannealed, 300 and 600 °C annealed copper oxides.

The FTIR spectrum of the copper oxide nanoparticles is shown in

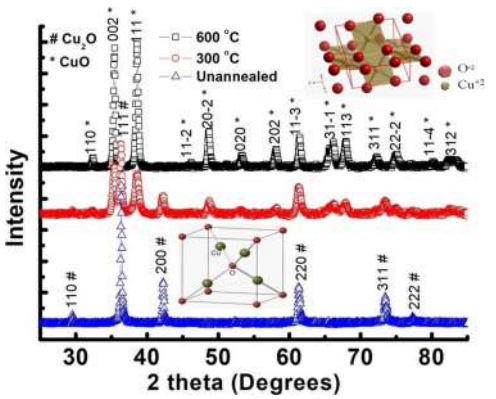


**Fig. 1.** XRD pattern of the copper oxide nanoparticles.

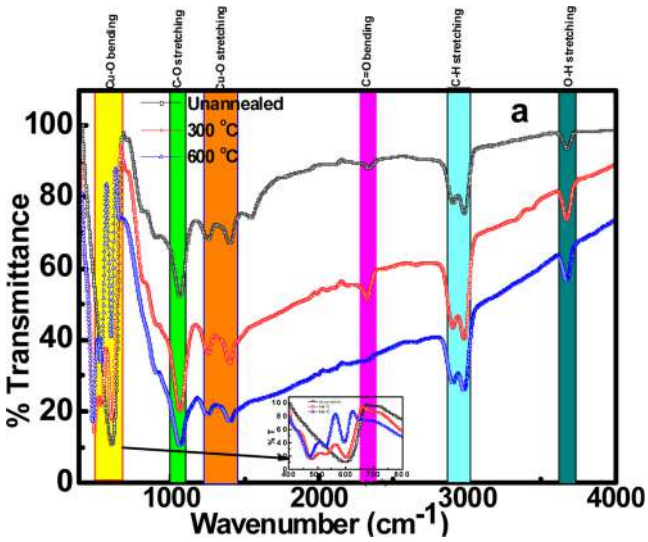


**Fig. 2.** ATR-FTIR spectrum of the copper oxide nanoparticles.

Fig. 2. The copper oxide annealed at 600 °C showed bands corresponding to the different bending vibration mode of the Cu-O at 471 and 520 cm$^{-1}$ (highlighted yellow) while the stretching band is at 1383 cm$^{-1}$ (highlighted orange). The band at 1047 cm$^{-1}$ is due to $ONO_2$ stretching (highlighted green) [41]. Similar peaks are seen in the 300 °C annealed copper oxides with slight shifts in the peak positions. The absence of the vibration mode peaks of Cu-O and the presence of the broad band around 600 cm$^{-1}$ in the unannealed copper oxide corresponds to absorption from $Cu_2O$ [42]. The bands at 2882-2963 cm$^{-1}$ (highlighted light blue green) and 3590-3650 cm$^{-1}$ (highlighted dark blue green) correspond to stretching vibrations from the C–H and the O—H bonds respectively [43]. The presence of the O—H stretching is due to absorption of atmospheric moisture by the copper oxide nanoparticles.

### 3.2. Optical properties

The absorbance spectrum of the dry husk extract is shown in Fig. 3a revealing an absorption peak at 226 nm and a broad peak around 325 nm. These peaks are due to the presence of flavonoids and its derivatives. The absorption spectra of flavonoids have been shown to typically consist of two absorption peaks in the ranges 230–285 nm (band I) and 300–380 nm (band II) ([44] [45],). Band I is considered to be associated with absorption due to the A-ring benzoyl system, while Band II occurs due to absorption involving the B-ring cinnamoyl system [46]. The diffuse reflectance is shown in Fig. 3b. The un-annealed copper oxide nanoparticles showed high reflectance and some absorption peaks in the infrared region. This absorption peak is because of the presence of organic plant extracts still present in the sample. There was a drastic decrease in the reflectance after annealing at 300 °C, and the absorption peaks in the infrared region disappeared indicating that the organic plant extracts has burnt off. The sample annealed at 600 °C absorbs highly in the visible region, an indication of a good solar absorber material and good photocatalytic activity. The bandgap energy was estimated from the diffuse reflectance by using the Kubelka-Munk function [47]. The estimated bandgap energy is 2.0, 1.30 and 1.42 eV respectively for the unannealed, 300 °C and 600 °C annealed copper oxide nanoparticles. There is a blue shift in energy for the annealed copper oxides in comparison to the bulk CuO bandgap (1.2 eV). Such blue shifts, which occur due to quantum size effects, have been reported for CuO nanostructures synthesized by various methods [27,48,49].

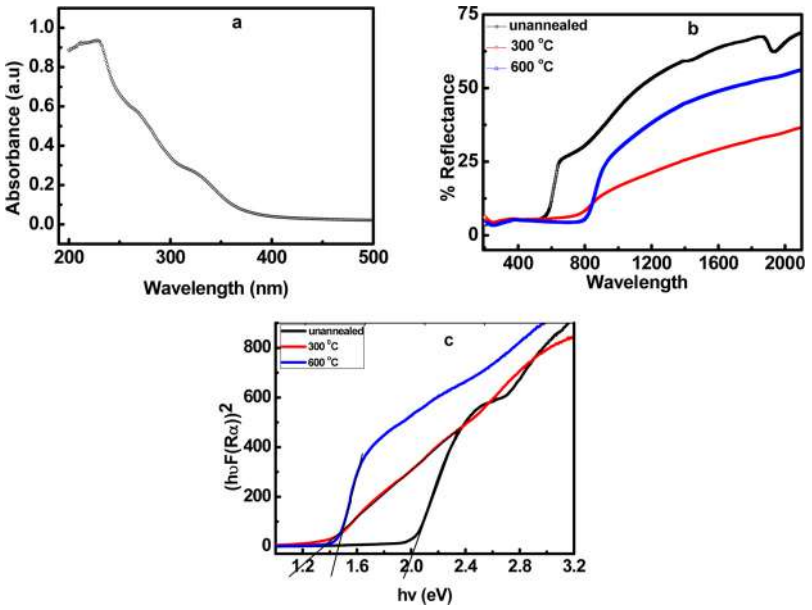


**Fig. 3.** Optical properties (a) absorption spectrum of the dry Husk extract (b) diffuse reflectance of the copper oxide nanoparticles (c) bandgap energy plot.

### *3.3. Morphological and elemental analysis*

The scanning electron microscopic images of the nanoparticles is shown in Fig. 4. The figure (Fig. 4a) reveals that the unannealed copper oxide nanoparticles consists of spherical and conical shaped agglomerates of the nanoparticles. On annealing at 300 °C (Fig. 4b), the agglomerates are broken down revealing pseudo spherical shaped nanoparticles of varying sizes. At 600 °C there is further breakdown of the agglomerates revealing a mix of big and small spherical nanoparticles. It obvious that annealing improves the crystallinity of the nanoparticles leading to well defined shapes.

Fig. 5 shows the high resolution transmission electron microscopy (HRTEM) images of the copper oxide nanoparticles. The unannealed copper oxide nanoparticles (Fig. 5a) consists of an agglomeration of spherical nanoparticles. The particle size distribution as shown in Fig. 5c indicates that the diameter of the nanoparticles range from 10 to 26 nm. The HRTEM of a singular nanoparticle as shown in Fig. 5b reveals a series of distinguishable planes with approximate $d_{hkl}$ distances of 0.24 nm and 0.34 nm. These values corresponds respectively to the (111) and (101) planes of the $Cu_2O$ cubic nanoparticle. The 300 °C annealed copper oxide nanoparticle (Fig. 6a) reveals nanorodlike particles with uneven length and width interspersed with some quasi spherical nanoparticles ranging between 36 to 73 nm. The HRTEM of a single nanorod indicates $d_{hkl}$ spacing of about 0.26 nm corresponding to the (002) diffraction plane of the CuO nanoparticle. The HRTEM of the 600 °C annealed copper oxide nanoparticles (Fig. 7a) consists of spherical nanoparticles with diameter in the range of 30 −90 nm (Fig. 7d). Fig. 7b reveals distinguishable reticular planes with approximate $d_{hkl}$ distances of 0.46 nm.

The selected area electron diffraction (SAED) profile of the copper oxide nanoparticles by its bright spots indicates the highly crystalline nature of the nanoparticles. The SAED of the annealed copper oxides

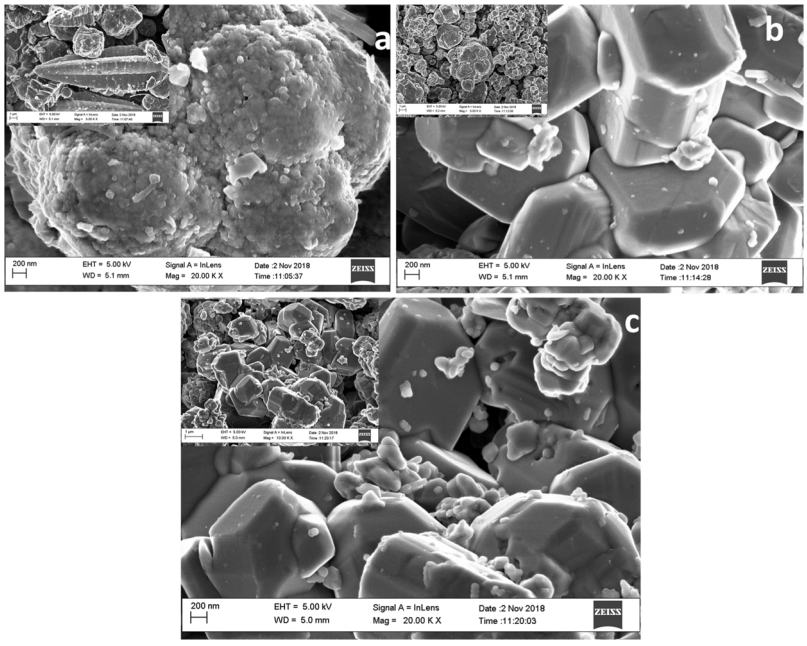


**Fig. 4.** SEM images of the copper oxide nanoparticles (a) unannealed (b) 300 °C (c) 600 °C.

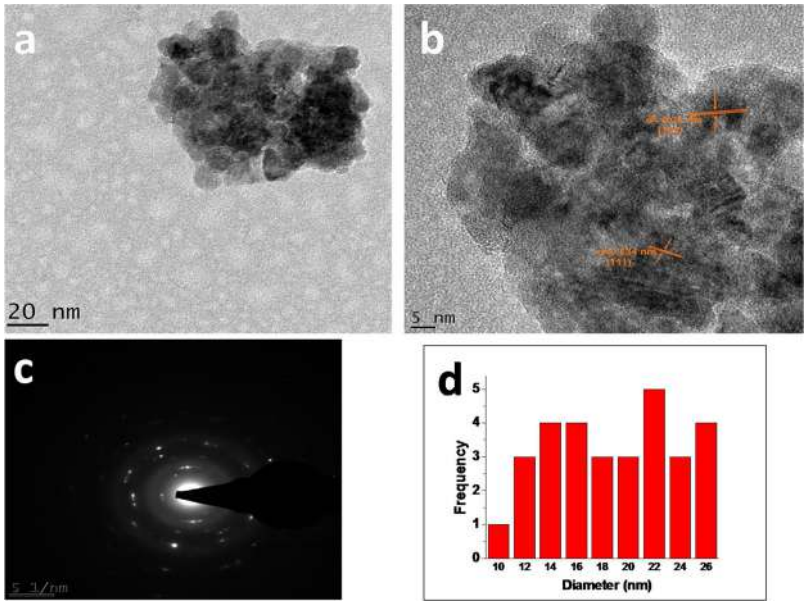


**Fig. 5.** (a) HRTEM image of the unannealed copper oxide particles (b) HRTEM image of a single nanoparticle (c) SAED pattern (d) particle size distribution.

(Figs. 6c and 7 c) reveals scattered bright spots arising from bragg reflections from the individual crystallites. It also corresponds with the many peaks observed in XRD data, compared to the unannealed copper oxide particles. All these lend credence to the polynanocrystalline nature of the nanoparticles.

The difference between the crystallite sizes obtained using the XRD peak FWHM and that obtained using TEM is because XRD gives average volume or domain sizes, which could consists of agglomeration of various nanoparticles in different orientations while TEM gives the size of individual particles. The values obtained using TEM is often considered more accurate. We can deduce from our result that annealing reduces or removes the agglomerations and results in Oswald ripening by which larger particles grow bigger at the expense of smaller particles.

The Energy Dispersive X-Ray Spectroscopy (EDS) spectra of all the nanoparticles (Fig. 8(a–c)) reveal the presence of copper and oxygen with insignificant traces of phosphorous in the 300 °C and 600 °C annealed samples. The latter elements came from the organic extract used as shown in Fig. 8d. The nickel and carbon peak is from the carbon coated nickel support grid used in the EDS analysis of copper oxide nanoparticles while a copper grid was used for the dry husk extract. The EDS of the dry husk extract reveals the presence of various elements such as phosphorous, magnesium, silicon, calcium, potassium, sulphur, carbon, and oxygen at various energy levels. However, the same silicon peak was observed when an area without the dry husk was analysed (spectrum not shown here), the silicon peak observed in the dry husk spectrum is in fact a spectral artefact/escape peak and therefore not a constituent of the dry husk [50].

### 3.4. Photocatalytic activity

Fig. 9 shows the degradation rates of TE and BM after 150 min, with

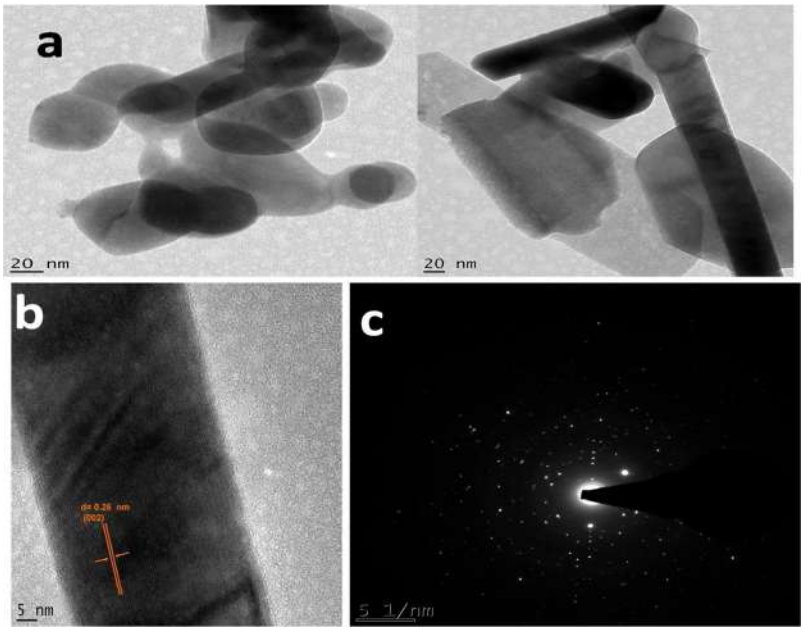


**Fig. 6.** (a) HRTEM image of the 300 °C annealed copper oxide nanoparticles (b) HRTEM image of a single nanoparticle (c) SAED pattern.

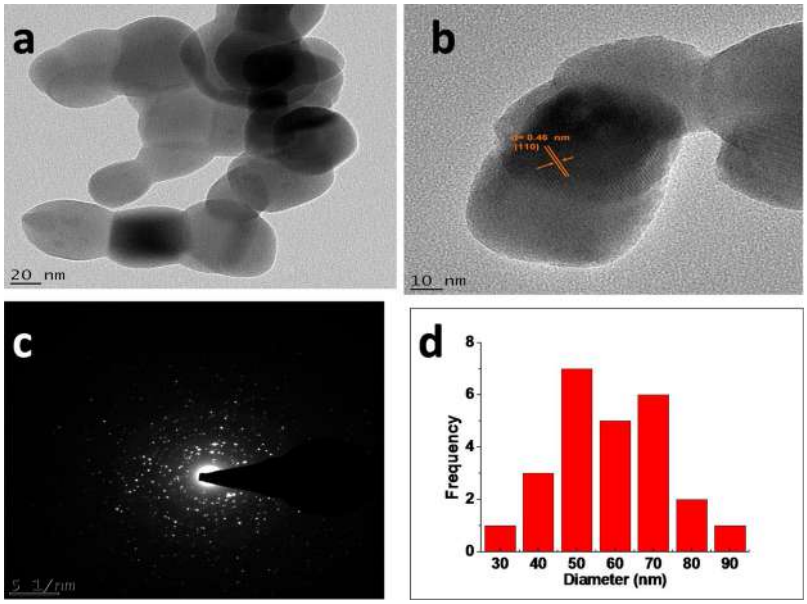


**Fig. 7.** (a) HRTEM image of the 600 °C annealed copper oxide nanoparticles (b) HRTEM image of a single nanoparticle (c) SAED pattern (d) particle size distribution.

and without CuO NPs contact time under visible light irradiation. The photocatalytic performance of the CuO NPs depends on the CuO type and the wastewater tested. In the presence of the visible light only, the BM and TE degradation rate is 37% and 2%, respectively. In contact with the CuO NPs, the TE and BM degradation increased up to 99% for the mixture of the three copper oxide NPs with each dye TE and BM. This high degradation rate obtained for the mixture of the three copper oxides could be due to generation of more electro-hole pairs and reduction in the electron-hole recombination rate. CuO is a p-type semiconductor with a narrow band gap of 1.3–1.6 eV [51]. Its conduction band and valence band are lower than the corresponding bands of $Cu_2O$ [52]. Therefore, the Cu2O + CuO_300 + CuO_600 forms a heterostructure type II staggered band structure and favoured charge transfer resulting in improved photocatalytic activities [53]. The dye removal efficiency increased to 80%, 87% and 91% for the BM wastewater in contact with $Cu_2O$, CuO_300 and CuO_600, respectively, and to 83%, 86% and 90% for the TE wastewater in the presence of the $Cu_2O$, CuO_300 and CuO_600, respectively. The lower degradation efficiency observed for the CuO_300, with a bandgap energy less than that of CuO_600 is most likely due to electron-hole recombination. The XRD result shows the presence of $Cu_2O$ in the CuO_300. Studies [54], have shown that pure $Cu^{2+}$ traps the photogenerated electrons while the reduced form also traps the hole thereby preventing electron hole recombination. This consequently leads to higher degradation efficiency. Secondly, we could also infer, based on our TEM results that the photocatalytic activity increases with increase in the nanoparticle sizes. The 91% degradation for the BM, which was obtained using CuO_600, is higher than the value (77%) obtained by Das et al., [55], using *Madhuca longifolia* plant mediated bio synthesized CuO. It is also higher than that (80%) achieved by Raizada et al. [56] using CuO prepared by solution combustion method. This shows the effectiveness of our zea mays mediated bio synthesized copper oxide nanoparticles towards human and environmental protection.

The absorbance of TE and BM wastewater under photocatalytic

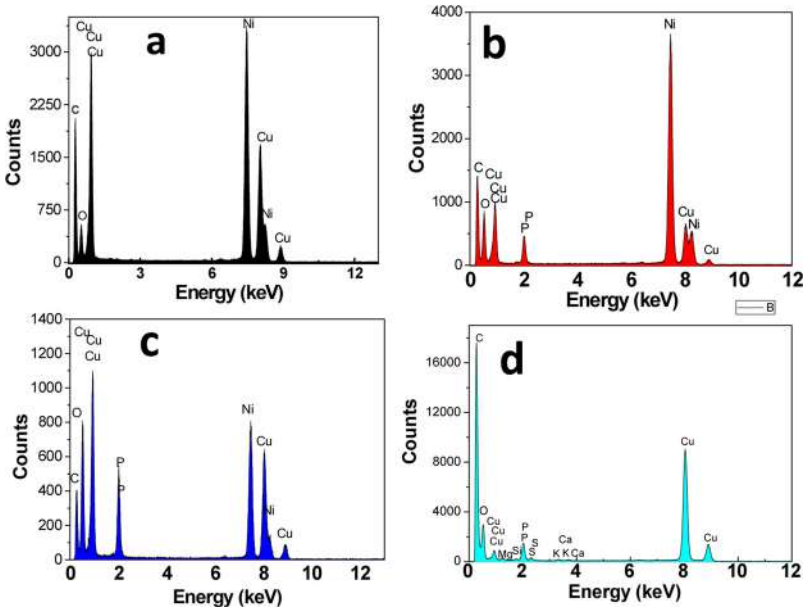


**Fig. 8.** EDS spectrum of the nanoparticles (a) unannealed (b) 300 °C(c) 600 °C and (d) the dry husk extract.

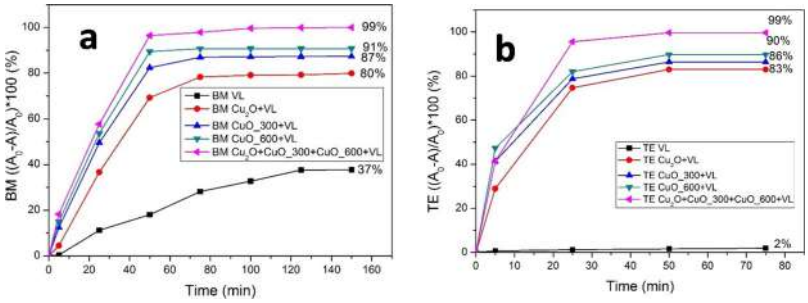


**Fig. 9.** Photocatalytic degradation of (a) Methylene blue (BM) and (b) Textile industrial effluent (TE). (For interpretation of the references to colour in this figure legend, the reader is referred to the web version of this article.)

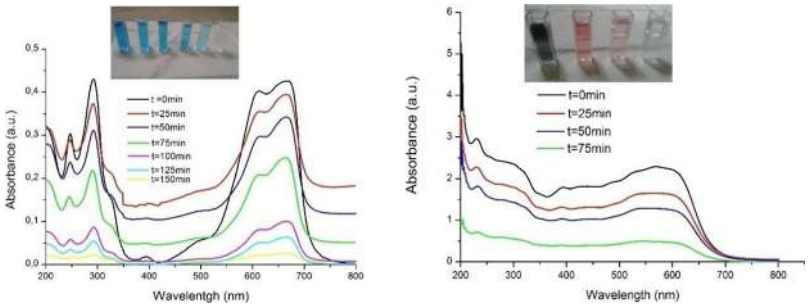


**Fig. 10.** Photocatalytic degradation of (A) Methylene blue and (B) Industrial textile effluent in contact time with CuO_600. (For interpretation of the references to colour in this figure legend, the reader is referred to the web version of this article.)

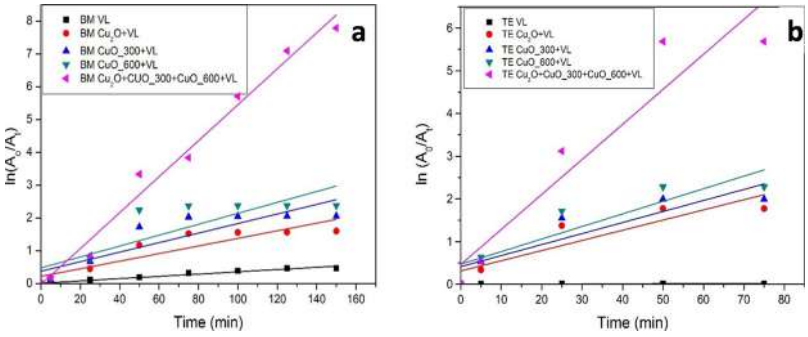


**Fig. 11.** Removal kinetics of the photocatalytic degradation of (a) Methylene blue (BM) and (b) Textile industrial effluent (TE) under visible light irradiation. (For interpretation of the references to colour in this figure legend, the reader is referred to the web version of this article.)

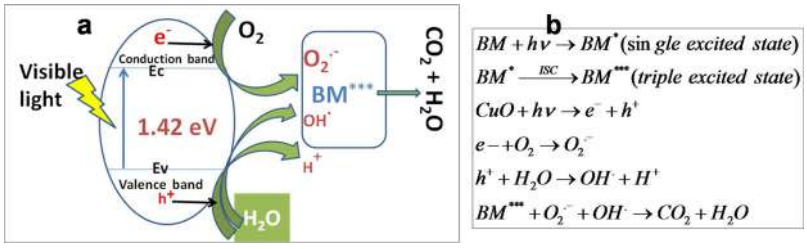


**Fig. 12.** (a) and (b) pictorial and schematic representation of the photocatalytic mechanism in the CuO_600.

activity of CuO NPs was measured between 200–800 nm every sampling time (Fig. 10). The dye degradation marked by the colour variation (from blue to white for BM wastewater and from dark brown to white for TE wastewater) was followed at 661 nm in the visible range. The basic condition of the medium with a pH above 7 avoids the formation of positive charge due to the presence of hydronium ions. The positive charge could reduce the performance of the active surface of the CuO NPs. The peak level decreased with the contact time with CuO NPs. Flat curves were obtained after 150 min., which means the complete degradation of the dyes. Further confirmation was obtained by the formation of the white colour.

### 3.4.1. Removal kinetics of BM and TE wastewater

The photocatalytic degradation follows the pseudo first order mechanism (Fig.11). The constant rate k value increases with the photocatalytic performance of each CuO NPs. The $Cu_2O$, CuO_300, CuO_600 and the mixture $Cu_2O$ + CuO_300 + CuO_600 nanoparticles have respectively a k value of 0.0238; 0.02582, 0.02944 and 0.08199 $min^{-1}$ ($R^2 > 0.8$).The visible light effect on the dye TE and BM degradation was very low with a k value of 0.0002 $min^{-1}$. This further indicates the

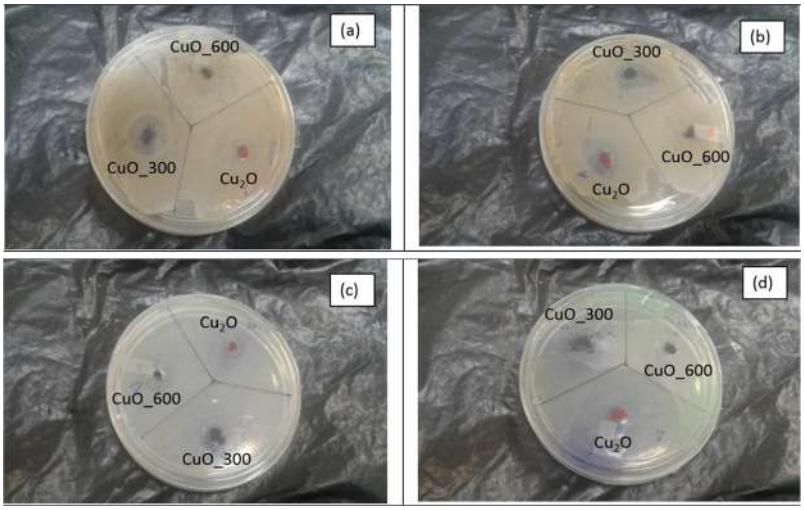


**Fig. 13.** Anti-bacterial effectiveness of the copper oxide nanoparticles against (a) *Escherichia coli* 518133 (b) *Staphylococcus aureus* 9144 (c) *Pseudomonas aeruginosa* and (d) *Bacillus licheniformis*.

high photocatalytic capabilities of our bio synthesized copper oxide nanoparticles.

The photocatalytic activity mechanism of the copper oxide nanoparticles (CuO_600) in the BM contaminated wastewater is shown pictorially in Fig. 12a. The BM absorbs photons of energy to get to the single excited state ($BM^{*}$). The $BM^{*}$ gets excited to the triple excited state ($BM^{***}$) as it undergoes intersystem crossing (ISC) [57]. With the absorption of photons of energy that is greater or equal to the bandgap energy of the copper oxide nanoparticles, electron hole pairs are created with the electron moving to the conduction band while the holes (or absence of electron) exist in the valence band. The excited electron moves from the conduction band and reacts with the dissolved oxygen species to form an oxide radical ion $O_2^{\cdot -}$. The hole ($h^+$) abstracts an electron from the hydroxyl ion (OH-) in water to generate a free radical OH·. The free radical ions react with the triple excited BM to yield the degradation products ($CO_2$ and $H_2O$) [55,57].

### 3.5. CuO antibacterial activity

The antibacterial effectiveness of each CuO NPs was evaluated as shown in Fig. 13. The inhibition zones have a diameter from 08 mm to 15 mm. CuO_300 had the largest diameter (15 mm) among all CuO NPs type. $Cu_2O$ and CuO_600 have respectively an inhibition zone diameter 10 mm and 7 mm. CuO_300 and $Cu_2O$ were very effective to inhibit the growth of *Escherichia coli* 518,133 and *Staphylococcus aureus 9144* (Fig. 13 (a) and (b)). For *Pseudomonas aeruginosa* and *Bacillus licheniformis* (Fig. 13(c) and (d)), $Cu_2O$ had an effect more visible than the two other types. CuO_300 is recommended to use to inhibit the growth of *Escherichia coli* 518,133 and *Staphylococcus aureus* 9144 and $Cu_2O$ is for *Pseudomonas aeruginosa* and *Bacillus licheniformis*.

## 4. Conclusion

Aqueous *Zea mays L.*dry husk extract was successfully used to obtain bio synthesized copper oxide nanoparticles. The absorption peaks obtained from the aqueous *Zea mays L.*dry husk extract are characteristic for flavonoids and its derivatives while the various elements presented were identified by EDS. Pure reddish cubic $Cu_2O$ nanoparticles were obtained for the first time, which were thermally oxidized to pure monoclinic CuO nanoparticles at 600 °C. The effectiveness of the copper oxide nanoparticles towards photodegradation of wastewater and anti microbial activity is confirmed. 91% and 90% degradation for BM and TE wastewater respectively were obtained using CuO_600. While CuO_600 is more effective to inhibit the growth of *Escherichia coli* 518133 and *Staphylococcus aureus 9144*, $Cu_2O$ is better for *Pseudomonas aeruginosa* and *Bacillus licheniformis*.

## Acknowledgement

This research was generously supported through the research funding from UNESCO UNISA Africa Chair in Nanosciences/ Nanotechnology, College of Graduate Studies, University of South Africa (UNISA), Muckleneuk Ridge, Pretoria, South Africa, (Post-Doctoral Fellowship program under contract number:90406558). We are also grateful to Nanosciences African network (NANOAFNET), Materials Research Department (MRD), iThemba LABS-National Research Foundation (NRF), SomersetWest, SouthAfrica, SensorLab, (Department of Chemistry), and the Electron Microscope Unit, University of the Western Cape, South Africa.

## References

[1] World Health Organisation- Drinking Water, http://www.who.int/news-room/fact-sheets/detail/drinking-water, assessed 13/10/2018.
[2] P. Sivakumar, P.N. Palanisamy, Low-cost non-conventional activated carbon for the removal of reactive red 4: kinetic and Isotherm Studies, Rasayan J. Chem. 1 (4) (2008) 871–883.
[3] V. Ponnusami, S. Vikram, S.N. Srivastava, Guava (Psidium guajava) leaf powder: novel adsorbent for removal of methylene blue from aqueous solutions, J. Hazard. Mater. 152 (2008) 276–286.
[4] K.A. Tan, N. Morad, J.Q. Ooi, Phytoremediation of methylene blue and methyl orange using Eichhornia crassipes, Int. J. Environ. Sci. Technol. (Tehran) 7 (2016) 724–728.
[5] L.C. Razanamahandry, H. Karoui, H.A. Andrianisa, H. Yacouba, Bioremediation of soil and water polluted by cyanide: a review, Afr. J. Environ. Sci. Tech. 11 (6) (2017) 272–291.
[6] L.C. Razanamahandry, H.A. Andrianisa, H. Karoui, H. Yacouba, Cyanide dynamics in catchment areas affected by artisanal gold mining in Burkina Faso, Artisanal Small Mining Conference Proceedings 2018 (2018).
[7] C. Parvathi, U.S. Shoba, C. Prakash, S. Sivamani, Manihot esculenta peel powder: effective adsorbent for removal of various textile dyes from aqueous solutions, J. Test. Eval. 46 (6) (2018) 1–13.
[8] D. Mohan, A. Sarswat, Y.S. Ok, C.U. Pittman Jr, Organic and inorganic contaminants removal from water with biochar, a renewable, low cost and sustainable adsorbent – a critical review, Bioresour. Technol. 160 (2014) 191–202.
[9] A.K. Verma, R.R. Dash, P. Bhunia, A review on chemical coagulation/flocculation technologies for removal of colour from textile wastewaters, J. Environ. Manage. 93 (1) (2012) 154–168.
[10] C. Allegre, M. Maisseu, F. Charbit, P. Moulin, Coagulation–flocculation–decantation of dye house effluents: concentrated effluents, J. Hazard. Mater. 116 (1–2) (2004) 57–64.
[11] S.K. Nataraj, K.M. Hosamani, T.M. Aminabhavi, Nanofiltration and reverse osmosis thin film composite membrane module for the removal of dye and salts from the simulated mixtures, Desalination 249 (1) (2009) 12–17.
[12] L.Y. Lee, H.Y. Ng, S.L. Ong, J.Y. Hu, G.T.K. Kekre, B. Viswanath, W. Lay, H. Seah, Ozone-biological activated carbon as a pretreatment process for reverse osmosis

brine treatment and recovery, Water Res. 43 (16) (2009) 3948–3955.
[13] X. Wang, Y. Lou, X. Ye, X. Chen, L. Fang, Y. Zhai, Y. Zheng, C. Xiong, Efficient removal of heavy metal ions by forward osmosis membrane with a polydopamine modified zeolitic imidazolate framework incorporated selective layer, J. Hazard. Mater. 364 (2019) 339–348.
[14] V. Smita, V. Kumar, R.Q. Abdur, Dye decomposition by combined ozonation and anaerobic treatment: cost effective technology, J. Appl. Res. Technol. 15 (4) (2017) 340–345.
[15] U.S. Environmental Protection Agency, National Primary Drinking Water Regulations. U.S. EPA, Office of Water, Retrieved November 25, 2010 from (2008) http://water.epa.gov/drink/contaminants/index.cfm.
[16] S. Zinatloo-Ajabshir, Z. Salehi, M. Salavati-Niasari, Green synthesis and characterization of $Dy_2Ce_2O_7$ ceramic nanostructures with good photocatalytic properties under visible light for removal of organic dyes in water, J. Clean. Prod. 192 (2018) 678–687.
[17] M. Eghbali-Arani, A. Sobhani-Nasab, M. Rahimi-Nasrabadi, F. Ahmadi, S. Pourmasoud, Ultrasound-assisted synthesis of $YbVO_4$ nanostructure and $YbVO_4$/$CuWO_4$ nanocomposites for enhanced photocatalytic degradation of organic dyes under visible light, Ultrason. Sonochem. 43 (2018) 120–135.
[18] A. Mohamed, R. El-Sayed, T.A. Osman, M.S. Toprak, M. Muhammed, A. Uheida, Composite nanofibers for highly efficient photocatalytic degradation of organic dyes from contaminated water, Environ. Res. 45 (2016) 18–25.
[19] X. Fuku, N. Matinise, M. Masikini, K. Kasinathan, M. Maaza, An electrochemically active green synthesized polycrystalline NiO/MgO catalyst: use in photo-catalytic applications, Mater. Res. Bull. 97 (2018) 457–465.
[20] S. Chae, T. Noeiaghaei, Y. Oh, I.S. Kim, J.-S. Park, Effective removal of emerging dissolved cyanotoxins from water using hybrid photocatalytic composites, Water Res. 149 (2019) 421–431.
[21] M. Suleiman, M. Mousa, A.I.A. Hussein, Wastewater disinfection by synthesized copper oxide nanoparticles stabilized with surfactant, J. Mater. Environ. Sci. 6 (7) (2015) 1924–1937.
[22] M.N. Asl, N.M. Mahmodi, P. Teymouri, B. Shahmoradi, R. Rezaee, A. Maleki, Adsorption of organic dyes using copper oxide nanoparticles: isotherm and kinetic studies, J. Desalin. Water Treat. 57 (52) (2016) 25278–25287.
[23] K.J. McDonald, B. Reynolds, K.J. Reddy, Intrinsic properties of cupric oxide nanoparticles enable effective filtration of arsenic from water, Sci. Rep. 5 (2015) 11110.
[24] M. Salavati-Niasari, F. Davar, Synthesis of copper and copper(I) oxide nanoparticles by thermal decomposition of a new precursor, Mater. Lett. 63 (15) (2009) 441–443 3–4.
[25] A.A. Anber, M.S. Essa, G.A. Kadhim, S.S. Hashim, Preparation of nanoparticles copper oxide using an atmospheric-pressure plasma jet, J. Phys. Conf. Ser. 1032 (conference 1) (2018).
[26] I.M.S. Araújo, R.R. Silva, G. Pacheco, W.R. Lustri, A. Tercjak, J. Gutierrez, J.R.S. Júnior, F.H.C. Azevedo, G.S. Figuêredo, M.L. Vega, S.J.L. Ribeiro, H.S. Barud, Hydrothermal synthesis of bacterial cellulose–copper oxide nanocomposites and evaluation of their antimicrobial activity, Carbohydr. Polym. 179 (1) (2018) 341–349.
[27] C. Zhu, M.J. Panzer, Seed layer-assisted chemical bath deposition of cuo films on ito coated glass substrates with tunable crystallinity and morphology, Chem. Mater. 26 (2014) 2960–2966.
[28] S. Lee, H. Ryu, W.-J. Lee, J.-S. Bae, Effects of ammonia in the synthesis of copper (II) oxide nanostructures grown via microwave chemical bath deposition, Surf. Coat. Technol. 334 (2018) 438–443.
[29] A.C. Nwanya, D. Obi, K.I. Ozoemena, R.U. Osuji, C. Awada, A. Ruediger, M. Maaza, F. Rosei, F.I. Ezema, Facile synthesis of nanosheet-like cuo film and its potential application as a high-performance pseudocapacitor electrode, Electrochim. Acta 198 (2016) 220–230.
[30] R. Katwal, H. Kaur, G. Sharma, M. Naushad, D. Pathania, Electrochemical synthesized copper oxide nanoparticles for enhanced photocatalytic and antimicrobial activity, J. Ind. Eng. Chem. 31 (25) (2015) 173–184.
[31] M.I. Nabila, K. Kannabiran, Biosynthesis, characterization and antibacterial activity of copper oxide nanoparticles (CuO NPs) from actinomycetes, Biocatal. Agric. Biotechnol. 15 (2018) 56–62.
[32] M. Aminuzzaman, L.M. Kei, W.H. Liang, Green synthesis of copper oxide (CuO) nanoparticles using banana peel extract and their photocatalytic activities, AIP Conf. Proc. 1828 (2017) 020016.
[33] R. Sivaraj, P.K.S.M. Rahman, P. Rajiv, S. Narendhran, R. Venckatesh, Biosynthesis and characterization of Acalypha indica mediated copper oxide nanoparticles and evaluation of its antimicrobial and anticancer activity, Spectrochim. Acta A. Mol. Biomol. Spectrosc. 129 (14) (2014) 255–258.
[34] Y. Yu, Z. Fei, J. Cui, B. Miao, Y. Lu, J. Wu, Biosynthesis of copper oxide nanoparticles and their in vitro cytotoxicity towards nasopharynx Cancer (KB cells) cell lines, Int. J. Pharmacol. 14 (2018) 609–614.
[35] S.M. Selvan, K.V. Anand, K. Govindaraju, S. Tamilselvan, V.G. Kumar, K.S. Subramanian, M. Kannan, K. Raja, Green synthesis of copper oxide nanoparticles and mosquito larvicidal activity against dengue, zika and chikungunya causing vector Aedes aegypti, IET Nanobiotechnol (2018) 8, https://doi.org/10.1049/iet-nbt.2018.5083.
[36] A. Brobbey, S. Somuah-Asante, S. Asare-Nkansah, F.O. Boateng, I. Ayensu, Preliminary phytochemical screening and scientific validation of the anti-diabetic effect of the dried husk of Zea mays L. (Corn, Poaceae), Int. J. Phytopharm. 7 (1) (2017) 01–05.
[37] K.-B. Roh, H. Kim, S. Shin, Y.-S. Kim, J.-A. Lee, M.O. Kim, E. Jung, J. Lee, D. Park, Anti-inflammatory effects of Zea mays L. husk extracts, BMC Complement, Altern. Med. 16 (2016) 298.
[38] X. Tang, X. Zhang, H. Zhang, X. Zhuang, X. Yan, Corn husk for noise reduction: robust acoustic absorption and reduced thickness, Appl. Acoust. 134 (2018) 60–68.
[39] Y. Zhu, K. Mimura, M.M. Isshiki, Oxidation mechanism of $Cu_2O$ to CuO at 600–1050 °C, Oxid. Met. 62 (2004) 207–222.
[40] A.C. Nwanya, M.M. Ndipingwi, N. Mayedwa, L.C. Razanamahandry, C.O. Ikpo, T. Waryo, S.K.O. Ntwampe, E. Malenga, E. Fosso-Kankeu, F.I. Ezema, E.I. Iwuoha, M. Maaza, Maize (Zea mays L.) fresh husk mediated biosynthesis of copper oxides: potentials for pseudocapacitive energy storage, Electrochim. Acta 301 (2019) 436–448.
[41] V. Prakash, R.K. Diwan, U.K. Niyogi, Characterization of synthesized copper oxide nanopowder and their use in nanofluids for enhancement of thermal conductivity, Ind. J. Pure Appl. Phys. 53 (2015) 753–758.
[42] R. Sankar, P. Manikandan, V. Malarvizhi, T. Fathima, K.S. Shivashangari, V. Ravikumar, Green synthesis of colloidal copper oxide nanoparticles using Carica papaya and its application in photocatalytic dye degradation, Spect. Acta Part A: Mol. Biomol. Spect. 121 (2014) 746–750.
[43] P.K. Raul, S. Senapati, A.K. Sahoo, I.M. Umlong, R.R. Devi, A.J. Thakur, V. Veer, CuO nanorods: a potential and efficient adsorbent in water purification, RSC Adv. 4 (2014) 40580–40587.
[44] K. Kalaichelvi, S.M. Dhivya, Screening of phytoconstituents, UV-VIS Spectrum and FTIR analysis of Micrococca mercurialis (L.) Benth, Int. J. Herb. Med. 5 (6) (2017) 40–44.
[45] T.J. Mabry, K.R. Markham, M.B. Thomas, The ultraviolet spectra of flavones and flavonols, The Systematic Identification of Flavonoids, Springer, Berlin, Heidelberg, 1970.
[46] L. Jurd, T.A. Geissman (Ed.), the Chemistry of Flavonoid Compounds, Pergamon Press, Oxford, 1962, p. 107.
[47] O. Schevciw, W.B. White, The optical absorption edge of rare earth sesquisulfides and alkaline earth-rare earth sulfides, Mat. Res. Bull. 18 (1983) 1059–1068.
[48] H.-M. Xiao, S.-Y. Fu, L.-P. Zhu, Y.-Q. Li, G. Yang, Controlled synthesis and characterization of cuo nanostructures through a facile hydrothermal route in the presence of sodium citrate, Eur. J. Inorg. Chem. 14 (2007) 1966–1971.
[49] Q. Liu, H. Liu, Y. Liang, Z. Xu, G. Yin, Large-scale synthesis of single-crystalline CuO nanoplatelets by a hydrothermal process, Mater. Res. Bull. 41 (2006) 697–702.
[50] D.E. Newbury, Mistakes Encountered During Automatic Peak Identification of Minor and Trace Constituents in Electron-Excited Energy Dispersive X-Ray Microanalysis, Scanning vol. 31, Wiley Periodicals, Inc, 2009, pp. 91–101.
[51] K. Nakaoka, J. Ueyama, K. Ogura, Photoelectrochemical behavior of electrodeposited CuO and Cu2O thin films on conducting substrates, J. Electrochem. Soc. 151 (2004) 661–665.
[52] C. Morales-Guio, L. Liardet, M.T. Mayer, S.D. Tilley, M. Grätzel, X. Hu, Photoelectrochemical hydrogen production in alkaline solutions using Cu2O coated with earth-abundant hydrogen evolution catalysts, Angew. Chem. Int. Ed. 54 (2015) 664–667.
[53] D. Jiang, J. Xue, L. Wu, W. Zhou, Y. Zhang, X. Li, Applied Catalysis B : Environmental Photocatalytic performance enhancement of CuO / $Cu_2O$ heterostructures for photodegradation of organic dyes : effects of CuO morphology, "Applied Catal. B, Environ. 211 (2017) 199–204.
[54] M. Janczarek, E. Kowalska, On the origin of enhanced photocatalytic activity of copper-modified titania in the oxidative reaction systems, Catalysts 7 (2017) 317.
[55] P. Das, S. Ghosh, R. Ghosh, S. Dam, M. Baskey, Madhuca longifolia plant mediated green synthesis of cupric oxide nanoparticles: a promising environmentally sustainable material for waste water treatment and efficient antibacterial agent, J. Photochem Photobiol B189 189 (2018) (2018) 66–73 66–73.
[56] A. Raizada, D. Ganguly, M.M. Mankad, A highly efficient copper oxide nanopowder for adsorption of methylene blue dye from aqueous medium, J. Chem. Eng. Res. Updates 2 (1) (2014) 249–258.
[57] A. Shah, N. Mittal, V.K. Sharma, P.B. Punjabi, Photodegradation of two commercial dyes in aqueous phase using copper oxide as photocatalyst, Int. J. Chem. Sci. 7 (4) (2009) 2345–2353.